Model-Free Output Feedback Path Following Control for Autonomous Vehicle With Prescribed Performance Independent of Initial Conditions

Zhongchao Liang, Mingyu Shen, Zhongguo Li, *Member, IEEE*, and Jun Yang, *Fellow, IEEE*

***Abstract*—Time-delay control (TDC) is widely recognized as a robust and straightforward model-free control approach for complex systems. However, the transient performance and settling time are often given less consideration in most TDC-based controllers. In this article, we propose an integrated control protocol that combines fixed-time prescribed performance control with time-delay estimation techniques for autonomous ground vehicles. The proposed control paradigm offers the advantages of being model-free while ensuring that the preview error converges to a neighborhood of zero within a fixed time, adhering to predefined constraint functions. To overcome the limitations of commonly used exponential decay boundaries, a prescribed performance function that remains independent of the initial conditions is employed. Furthermore, a high-order model-free fixed-time differentiator is constructed to observe the high-order dynamics of the preview error, which are essential for estimating unknown model dynamics. Finally, the simulations and practical experiments have been conducted to demonstrate the superiority of our proposed control protocol.**

***Index Terms*—Fixed-time convergence, model free, path-following control, prescribed performance control (PPC), time-delay control (TDC).**

NOMENCLATURE

$\delta_{\rm f}$	Front-wheel steering angle.
β/γ	Sideslip angle/yaw rate of vehicle.
d_β/d_γ	Item incorporating uncertainties and disturbances in sideslip/yaw dynamics of vehicle.
$v_x/v_{\rm d}$	Actual/ideal longitudinal vehicle speed.
$l_{\rm f}/l_{\rm r}$	Distance from front/rear axle to center of gravity (CG).
$c_{\rm f}/c_{\rm r}$	Front/rear tire cornering stiffness.
$\Delta c_{\rm f}/\Delta c_{\rm r}$	Nonlinear component of front/rear tire cornering stiffness.
m	Vehicle mass.
I_Z	Vehicle's moment of inertia around Z-axis.
R	Effective wheel radius.
$F_{\rm fax}/F_{\rm rax}$	Total traction or braking force on front/rear wheels.
$F_{\rm fay}/F_{\rm ray}$	Total lateral force on front/rear wheels.
T_a	Total torque on all four wheels for driving or braking.
ΔT_i	Torque loss of wheel i during driving or braking, where i represents wheel number out of four wheels.
e/ψ	Lateral distance/bearing angle offset.
L	Preview length.
σ	Preview error, referring to distance offset between desired path and vehicle's preview point at preview length L.
s	Arc length of vehicle location.
$\kappa_s(s)$	Ideal curvature at arc length s.
k_ρ	Positive parameter for decay rate in prescribed performance boundary function.
k_∞	Ultimate boundary in prescribed performance boundary function, and $0 < k_\infty \ll 1$.
$\hat{\sigma}$, $\hat{\dot{\sigma}}$, $\hat{\ddot{\sigma}}$	Estimates of σ, $\dot{\sigma}$, and $\ddot{\sigma}$, respectively.
k_1, k_2, k_3	Positive estimate gains in second-order differentiator.
κ_1, κ_2, κ_3	Positive gains in composite terms of nonlinear output injection to construct bl-homogeneous system near origin.
θ_1, θ_2, θ_3	Positive gains in composite terms of nonlinear output injection to construct bl-homogeneous system near infinity.
k_y, k_ω	Positive control gains for proposed controller.
η_1, η_{11}, η_2, η_{22}	Positive gains for adaptive law.

Manuscript received 24 December 2022; revised 15 June 2023; accepted 3 July 2023. Recommended by Technical Editor S. Jeon and Senior Editor H. Fujimoto. This work was supported in part by the National Natural Science Foundation of China under Grant 51975109 and in part by the Fundamental Research Funds for the Central Universities under Grant N2103018. *(Corresponding author: Zhongguo Li.)*

Zhongchao Liang and Mingyu Shen are with the School of Mechanical Engineering and Automation, Northeastern University, Shenyang 110819, China (e-mail: liangzc@me.neu.edu.cn; shenmy@stumail.neu.edu.cn).

Zhongguo Li is with the Department of Computer Science, University College London, WC1E 6BT London, U.K. (e-mail: zhongguo.li@ucl.ac.uk).

Jun Yang is with the Department of Aeronautical and Automotive Engineering, Loughborugh University, LE11 3TU Loughborough, U.K. (e-mail: j.yang3@lboro.ac.uk).

Color versions of one or more figures in this article are available at https://doi.org/10.1109/TMECH.2023.3293100.

Digital Object Identifier 10.1109/TMECH.2023.3293100

I. Introduction

IN RECENT decades, autonomous driving for autonomous ground vehicles (AGVs) has emerged as a significant technology that aims to improve traffic safety, mobility, and driving comfort [1]. The path-following subsystem in an AGV plays a crucial role in following desired paths by controlling the vehicle's motions [2]. Consequently, it has become a focal point of recent research. However, due to the nonlinear dynamics of the vehicles, path-following control still presents numerous challenges in terms of automation [3], [4].

Various theories and methodologies have been investigated to stabilize the path-following error for AGVs, including model predictive control [5], H_∞ feedback control [6], and sliding mode control [7]. However, most existing approaches share a common requirement of complex model dynamics in controller design. The conventional path-following controller for AGVs relies on accurate vehicle dynamics models and related parameters, which are challenging to obtain in the real world [8]. To address this limitation, a promising alternative is the utilization of a model-free paradigm known as time-delay control (TDC). It employs the time-delay estimation (TDE) technique [9], which uses intentionally delayed signals to estimate the lumped system dynamics and introduces the model-free characteristic [10]. Consequently, TDC- and TDE-based controllers have been successfully employed to construct model-free controllers for AGVs [11], robot manipulators [12], and other nonlinear systems [13].

The transient performance and the settling time are of great significance for control performance but have received less attention in existing TDE-based research. To address the transient performance, the prescribed performance control (PPC) approach has been considered, aiming to limit the state error according to predefined performance constraints. This ensures that the control performance of the state error remains bounded throughout the control process, with the maximum overshoot constrained by a predefined boundary function [14]. Consequently, the PPC technique has been widely applied in path-following control systems of AGVs [15], [16]. However, existing PPC-based approaches typically utilize exponential decay functions as preset boundaries. This requirement implies that the initial condition must be known to satisfy the initial constraint, which contradicts the characteristics of the fixed-time control scheme, where the convergence rate is independent of the initial states. To accommodate various scenarios with different initial state errors, we introduce a prescribed performance boundary function that ensures complete independence of the initial conditions.

From another perspective, the convergence performance of a controlled system is characterized by the settling time [17], and achieving fast convergence is often desirable in practice. The settling time property can be classified into asymptotic, finite-time, and fixed-time convergences. Finite-time control algorithms, such as terminal sliding mode control, fall into the category of finite-time convergence, but their convergence rate depends on the initial system states [18]. In addition, fixed-time stability, an extension of the finite-time control scheme, ensures that the settling time remains uniformly bounded regardless of initial conditions [19]. Therefore, combining the fixed-time control and PPC approaches allows for the consideration of both steady-state and transient system behaviors.

This article presents a novel fixed-time prescribed performance and model-free (FTPPC-MF) control protocol for AGVs to achieve path following with prescribed performance. The main contributions of this article are stated as follows.

1) Unlike most existing TDC schemes [20], [21], our proposed FTPPC-MF control protocol restricts the preview error, which indicates the path-following performance, within a preset boundary. Unlike previous PPC-based schemes [10], [22], [23], our protocol does not require the initial state errors of the vehicle to establish initial boundaries. In addition, the integration of the fixed-time control algorithm ensures the fixed settling time independent of initial conditions.
2) To address the challenge of estimating unknown vehicle dynamics using the TDE technique, we introduce a fixed-time high-order differentiator into our controller. This differentiator estimates the high-order preview error dynamics by utilizing only the outputs of the controlled system, such as the vehicle location and posture. The proposed differentiator exhibits model-free and fixed settling time properties, enhancing the estimation accuracy of unknown dynamics.
3) We validate the effectiveness and superiority of our proposed FTPPC-MF protocol through simulations and practical vehicle experiments. The results demonstrate the enhanced path-following performance achieved by our control approach and highlight its potential for real-world applications.

The rest of this article is organized as follows. Section II presents the modeling and problem formulation. Section III introduces the design of the high-order differentiator and the path-following controller. Simulations and practical experiments are conducted in Sections IV and V, respectively. Finally, Section VI concludes this article.

II. Problem Formulation

A. Vehicle and Preview Error Dynamics

The lateral vehicle dynamics model commonly used can be expressed as follows [24]:

$$\begin{cases} \dot{\beta} = a_1\beta + a_2\gamma + b_1\delta_{\mathrm{f}} + d_\beta \\ \dot{\gamma} = a_3\beta + a_4\gamma + b_2\delta_{\mathrm{f}} + d_\gamma \end{cases} \tag{1}$$

in which the parameters are given by $a_1 = -\frac{c_{\mathrm{f}}+c_{\mathrm{r}}}{v_x m} - \frac{F_{\mathrm{fax}}+F_{\mathrm{rax}}}{mv_x} - \frac{\Delta c_{\mathrm{f}}+\Delta c_{\mathrm{r}}}{v_x m}$, $a_2 = -1 + \frac{l_{\mathrm{r}}c_{\mathrm{r}}-l_{\mathrm{f}}c_{\mathrm{f}}}{mv_x^2} + \frac{l_{\mathrm{r}}\Delta c_{\mathrm{r}}-l_{\mathrm{f}}\Delta c_{\mathrm{f}}}{mv_x^2}$, $a_3 = \frac{l_{\mathrm{r}}c_{\mathrm{r}}-l_{\mathrm{f}}c_{\mathrm{f}}}{I_Z} + \frac{l_{\mathrm{r}}\Delta c_{\mathrm{r}}-l_{\mathrm{f}}\Delta c_{\mathrm{f}}}{I_Z}$, $a_4 = -\frac{l_{\mathrm{f}}^2c_{\mathrm{f}}+l_{\mathrm{r}}^2c_{\mathrm{r}}}{I_Z v_x} - \frac{l_{\mathrm{f}}^2\Delta c_{\mathrm{f}}+l_{\mathrm{r}}^2\Delta c_{\mathrm{r}}}{I_Z v_x}$, $b_1 = \frac{c_{\mathrm{f}}}{v_x m}$, and $b_2 = \frac{l_{\mathrm{f}}c_{\mathrm{f}}}{I_Z}$.

The primarily focus is on the lateral distance offset e and the bearing angle offset ψ between the vehicle and the desired path during path following. The dynamics of these error variables e

and ψ can be described as follows [24]:

$$\begin{cases} \dot{e} = v_x\psi + v_x\beta \\ \dot{\psi} = \gamma - \kappa_s(s)v_s \end{cases} \tag{2}$$

where $v_s = \frac{v_x}{1-e\kappa_s(s)}$.

The preview error σ has been widely used to evaluate the path-following performance by incorporating both e and ψ. It can be expressed as follows:

$$\sigma = e + L\psi. \tag{3}$$

Based on the dynamics of e and ψ in (2), the preview error dynamics can be calculated by considering the lateral vehicle dynamics (1) as follows:

$$\dot{\sigma} = v_x\psi + v_x\beta - L\kappa_s v_s + L\gamma \tag{4}$$

$$\ddot{\sigma} = h + b\delta_{\mathrm{f}} \tag{5}$$

where

$$\begin{aligned} h = {} & (\psi+\beta)\,\dot{v}_x - v_s v_x \kappa_s - L\kappa_s \dot{v}_s - L(\mathrm{d}\kappa_s/\mathrm{d}s)v_s^2 \\ & + v_x\left(a_1\beta + a_2\gamma\right) + L\left(a_3\beta + a_4\gamma\right) \\ & + \underbrace{(b_1 + b_2 L)}_{b\neq 0}\delta_{\mathrm{f}} + v_x d_\beta + L d_\gamma. \end{aligned}$$

In (5), the variable h represents the lumped time-varying path-following dynamics, which encompasses all nonlinearities and uncertainties. Due to its complexity and difficulty in accurate estimation in practical scenarios, the subsequent controller design will not incorporate the models of the vehicle dynamics (1) and the preview error dynamics (5).

Since path following primarily focuses on the lateral dynamics of the vehicle, we provide discussions on the longitudinal vehicle dynamics and the construction of the corresponding longitudinal speed controller in the Appendix section.

B. Control Objectives

To prescribe the transient and steady-state performance of the preview error, we propose the following time-varying constraints [25]:

$$I(-\Psi) < \sigma < I(\Psi) \tag{6}$$

where $I(\Psi)$ represents the time-varying prescribed function, defined as follows:

$$I(\Psi) = \frac{\sqrt{1-k_\infty^2}\Psi}{\sqrt{1-\Psi^2}} \tag{7}$$

with

$$\Psi(t) = (1-k_\infty)\exp\left(-k_\rho t\right) + k_\infty. \tag{8}$$

It is specifically ensured that $0 < k_\infty \ll 1$.

A steering controller is proposed to achieve the following objectives.

1) *Model-free feature:* The controller design does not rely on the knowledge of vehicle and path-following models or their associated parameters.
2) *Prescribed performance without initial constraint:* The preview error is constrained throughout the entire path-following process by the preset constraints defined in (6)
3) *Fixed settling time:* The preview error described in (3) is driven to a residual set of (6) within a fixed time.

Remark 1: Equation (8) represents an exponential decay function commonly used as the prescribed performance constraints in conventional PPC algorithms. It decays from 1 to k_∞ as time varies from 0 to ∞. In order to satisfy the initial constraints in conventional PPC algorithms, the initial system state error needs to be smaller than 1 or other values by multiplying a factor to (8). The parameter k_ρ represents the decay rate of the boundary function (8), whereas k_∞ represents the ultimate boundary. In our proposed transformed constraint function from (8) to (7) through a homeomorphism mapping, the decay boundary from 1 to k_∞ is transformed to a boundary from $+\infty$ to k_∞. As a result, the proposed boundary in (6) allows for an open initial boundary condition as follows:

$$\begin{cases} I(\Psi(0)) = I(1) = \infty \\ \lim_{t\to\infty} I(\Psi(t)) = I\left(k_\infty\right) = k_\infty. \end{cases} \tag{9}$$

However, it is important to note that the transformed function $I(\Psi)$ cannot be directly used in the controller due to the singularity at $t = 0$. This is different from the conventional PPC controller design process. We have taken this singularity issue into account and will address it in the subsequent controller design through the error transformation outlined in (37) and (38).

C. Preminaries

Lemma 1 (see [26]): Consider two single-valued, upper semicontinuous (u.s.c.), and homogeneous in the bilimit functions: $\phi : \mathbb{R}^n \to \mathbb{R}$ and $\xi : \mathbb{R}^n \to \mathbb{R}_{\leq 0}$. These two functions possess identical near zero weights vector, denoted as $\mathbf{g}_0$, near infinity weights vector, denoted as $\mathbf{g}_\infty$, near zero degrees, denoted as h_0, near infinity degrees, denoted as h_∞, as well as near zero approximating functions ϕ_0 with ξ_0, and near infinity approximating functions ϕ_∞ with ξ_∞. If, for $\iota \in \{0, \infty\}$, $\phi(z) < 0$ and $\phi_\iota(z) < 0$ can be obtained using $\xi(z) = 0 \wedge z \neq 0$ and $\xi_\iota(z) = 0 \wedge z \neq 0$, respectively, then there exists a real constant l^*, along with positive constants $l_0 > 0$ and $l_\infty > 0$, such that, for all $l \geq \max\{l_0, l_\infty\}$, $l_0 \geq l^*, l_\infty \geq l^*$ and $z \in \mathbb{R}^n \backslash \{0\}$,

$$\begin{aligned} & \phi(z) + l\xi(z) \leqslant -l_0 \parallel z \parallel_{\mathbf{g}_0,p}^{h_0} - l_\infty \parallel z \parallel_{\mathbf{g}_\infty,p}^{h_\infty} \\ & \phi_\iota(z) + l\xi_\iota(z) \leqslant -l_\iota \parallel z \parallel_{\mathbf{g}_\iota,p}^{h_\iota}, \quad \iota \in \{0, \infty\} \end{aligned} \tag{10}$$

where $\|z\|_{\mathbf{g}_\iota,p}^{h_\iota}$ represents the homogeneous norm that can be calculated by $(\sum_{i=1}^n |z_i|^{p/g_i})^{h_\iota/p}$; z_i and g_i represent the ith components of z and $\mathbf{g}_\iota$, respectively; p is a positive real number.

Lemma 2 (see [27]): Consider two continuous and homogeneous in the bilimit functions: $\phi : \mathbb{R}^n \to \mathbb{R}$ and $\xi : \mathbb{R}^n \to \mathbb{R}_{\geq 0}$ with same weights. The function ϕ (respectively, ξ) possesses the near zero degree $h_{\phi,0}$ (respectively, $h_{\xi,0}$), the near infinity degree $h_{\phi,\infty}$ (respectively, $h_{\xi,\infty}$), as well as the near zero approximating function ϕ_0 (respectively, ξ_0), and the near infinity approximating function ϕ_∞ (respectively, ξ_∞). If the conditions $h_{\phi,0} \geq h_{\xi,0}$ and $h_{\phi,\infty} \leq h_{\xi,\infty}$ with the positive definite functions ξ_0 and ξ_∞

are satisfied, then the following inequality holds for $k_z \in \mathbb{R}_{>0}$:

$$\phi(z) \leq k_z \xi(z) \quad \forall z \in \mathbb{R}^n. \tag{11}$$

Lemma 3 (see [28]): For $\forall a, b \in \mathbb{R}$, one has

$$ab \leq k^p p^{-1}|a|^p + k^q q^{-1}|b|^q \tag{12}$$

where $k > 0$; $p > 1$ and $q > 1$ satisfy $(p-1)(q-1) = 1$.

Lemma 4 (see [29]): For $a_i \geq 0, i = 1, \ldots, n$, the following inequalities hold:

$$\begin{aligned} \sum_{i=1}^{n} a_i^p &\geq \left(\sum_{i=1}^{n} a_i\right)^p, \quad 0 < p \leq 1 \\ \sum_{i=1}^{n} a_i^p &\geq n^{1-p}\left(\sum_{i=1}^{n} a_i\right)^p, \quad p > 1. \end{aligned} \tag{13}$$

Lemma 5 (see [29]): Consider a positive definite and radially unbounded function $V(x)$ for system $\dot{x} = f(x)$. If there exists

$$\dot{V} \leq -\alpha V^p - \beta V^q + C \tag{14}$$

where α, β, p, q, and C are positive bounded constants with $p > 1$ and $0 < q < 1$, then the system will converge to the following set with $0 < \gamma < 1$:

$$V(x) \leq V_{\max} = \min\left\{\left(\frac{C}{\alpha(1-\gamma)}\right)^{\frac{1}{p}}, \left(\frac{C}{\beta(1-\gamma)}\right)^{\frac{1}{q}}\right\} \tag{15}$$

within a fixed time T bounded by

$$T \leq T_{\max} = [\alpha\gamma(p-1)]^{-1} + [\beta\gamma(1-q)]^{-1}. \tag{16}$$

III. Controller Design

A. Observer for Preview Error Dynamics

In the subsequent controller design, it is necessary to have knowledge of the high-order dynamics of the preview error. While the preview error defined in (3) can be directly measured using the vehicle positioning system, obtaining the high-order dynamics of the preview error is not easily achievable with conventional sensors. To address this issue, we introduce the bl-homogeneous scheme, which is an approximation method that achieves homogeneous in the bilimit (bl-homogeneous) [26], [30]. This scheme allows us to approximate the real values of the high-order preview error dynamics in a fixed-time manner. Based on the bl-homogeneous scheme and a specific assumption (Assumption 1), the differentiators are constructed in Theorem 1.

Assumption 1: $\sigma(t)$ is three times differentiable and $|\dddot{\sigma}(t)| \leq M$ with a positive constant M.

Remark 2: Assumption 1 encompasses two key aspects. First, we assume that $\sigma(t)$ is three times differentiable to ensure the feasibility of formulating the estimate error dynamics for the second-order derivative of $\sigma(t)$, which is required for estimation in the constructed differentiator. Second, the boundedness of $\dddot{\sigma}(t)$ is necessary to provide evidence that the estimate error can converge to zero within a fixed time during the subsequent proof. In addition, the boundedness of $\dddot{\sigma}(t)$ can further deduce the results of uniform continuity for $\ddot{\sigma}(t)$. This, in turn, ensures the feedback continuity within the controlled system across the entire domain of $\ddot{\sigma}(t)$ when applied in the proposed controller. By ensuring feedback continuity, the controller maintains smooth and consistent control actions through the operation.

Theorem 1: Suppose the following differentiators:

$$\begin{aligned} \dot{\hat{\sigma}} &= -k_1\phi_1(\hat{\sigma} - \sigma) + \hat{\dot{\sigma}} \\ \dot{\hat{\dot{\sigma}}} &= -k_2\phi_2(\hat{\sigma} - \sigma) + \hat{\ddot{\sigma}} \\ \dot{\hat{\ddot{\sigma}}} &= -k_3\phi_3(\hat{\sigma} - \sigma) \end{aligned} \tag{17}$$

and the nonlinear output injection composite terms are given by

$$\begin{aligned} \phi_1(z) &= \varphi_1(\hat{\sigma} - \sigma) \\ \phi_2(z) &= \varphi_2(\varphi_1(\hat{\sigma} - \sigma)) \\ \phi_3(z) &= \varphi_3(\varphi_2(\varphi_1(\hat{\sigma} - \sigma))) \end{aligned} \tag{18}$$

with

$$\varphi_i(\cdot) = \kappa_i \lceil \cdot \rfloor^{\frac{r_{0,i+1}}{r_{0,i}}} + \theta_i \lceil \cdot \rfloor^{\frac{r_{\infty,i+1}}{r_{\infty,i}}}, \quad i = 1, 2, 3 \tag{19}$$

in which k_1, k_2, k_3, κ_1, κ_2, κ_3, θ_1, θ_2, and θ_3 are positive parameters as listed in the nomenclature section; $\lceil \cdot \rfloor^p = |\cdot|^p \operatorname{sign}(\cdot)$; the powers are selected as

$$\begin{aligned} &r_{0,1} = r_{0,2} - d_0, r_{\infty,1} = r_{\infty,2} - d_\infty \\ &r_{0,2} = r_{0,3} - d_0, r_{\infty,2} = r_{\infty,3} - d_\infty \\ &r_{0,3} = r_{\infty,3} = 1, r_{0,4} = 1 + d_0, r_{\infty,4} = 1 + d_\infty \end{aligned} \tag{20}$$

where $d_0 = -1$ and $-1 \leq d_\infty < \frac{1}{2}$. Then, $\hat{\sigma}$ and $\hat{\dot{\sigma}}$ will be driven to $\dot{\sigma}$ and $\ddot{\sigma}$, respectively, within a fixed time that can be estimated by

$$t_d \leq \frac{p_0}{\eta_\infty}\left(\frac{p_\infty}{p_0 d_\infty} + 1\right)\left(\frac{\eta_0}{\eta_\infty}\right)^{\frac{-1}{\left(\frac{p_\infty}{p_0 d_\infty} + 1\right)}}. \tag{21}$$

Proof: Define the estimate errors as $\tilde{\sigma}_1 \triangleq \hat{\sigma} - \sigma$, $\tilde{\sigma}_2 \triangleq \hat{\dot{\sigma}} - \dot{\sigma}$, and $\tilde{\sigma}_3 \triangleq \hat{\ddot{\sigma}} - \ddot{\sigma}$. Apply the following error transformations:

$$z_1 = \tilde{\sigma}_1, z_2 = \frac{\tilde{\sigma}_2}{k_1}, z_3 = \frac{\tilde{\sigma}_3}{k_2}. \tag{22}$$

Equation (22), together with (16) and $|\dddot{\sigma}(t)| \leq M$ in Assumption 1, yields

$$\begin{aligned} \dot{z}_1 &= -\tilde{k}_1(\phi_1(z_1) - z_2) \\ \dot{z}_2 &= -\tilde{k}_2(\phi_2(z_1) - z_3) \\ \dot{z}_3 &= -\tilde{k}_3\left(\phi_3(z_1) - \frac{\sigma^{(3)}(t)}{k_3}\right) \in -\tilde{k}_3\left(\phi_3(z_1) - \frac{M}{k_3}[-1, 1]\right) \end{aligned} \tag{23}$$

with $k_0 = 1$ and $\tilde{k}_i = \frac{k_i}{k_{i-1}}, i = 1, 2, 3$.

A smooth Lyapunov function for (23) is selected as

$$V(z) = V_1(z_1, z_2) + V_2(z_2, z_3) + V_3(z_3) \tag{24}$$

with

$$V_i(z_i, z_{i+1}) = \sum_{j\in\{0,\infty\}} \beta_{j,i}\left(\frac{r_{j,i}}{p_j}|z_i|^{\frac{p_j}{r_{j,i}}} - z_i\lceil\xi_i\rfloor^{\frac{p_j-r_{j,i}}{r_{j,i}}} + \frac{p_j - r_{j,i}}{p_j}|\xi_i|^{\frac{p_j}{r_{j,i}}}\right) \tag{25}$$

where $\xi_1 = \varphi_1^{-1}(z_2)$, $\xi_2 = \varphi_2^{-1}(z_3)$, and $\xi_3 = z_4 \equiv 0$; φ_1^{-1} and $\varphi_2^{-1}$are the inverse functions of φ_1 and φ_2, respectively; $\beta_{0,i}$ and $\beta_{\infty,i}$ for $i = 1, 2, 3$ are positive real numbers; $V_3(z_3) = \beta_{0,3}\frac{1}{p_0}|z_3|^{p_0} + \beta_{\infty,3}\frac{1}{p_\infty}|z_3|^{p_\infty}$.

Based on the definition of (25), V is $\mathcal{C}^1$ (continuously differentiable) on $\mathbb{R}$, and exhibits homogeneous in the bilimit with degrees p_0 and p_∞, respectively [30]. Furthermore, V is positive definite and radially unbounded.

Taking the time derivative of V and applying the dynamics (23) produce

$$\dot{V}(z) \in W(z) \tag{26}$$

$$W(z) = -\tilde{k}_1\vartheta_1\left[\phi_1(z_1) - z_2\right] - \tilde{k}_2(s_1 + \vartheta_2)\left[\phi_2(z_1) - z_3\right] - \tilde{k}_3(s_2 + \vartheta_3)\left[\phi_3(z_1) - \frac{M}{k_3}[-1, 1]\right] \tag{27}$$

where W is a u.s.c. set-valued function; $\vartheta_i \triangleq \frac{\partial S_i(z_i z_{i+1})}{\partial z_i}$ and $s_i \triangleq \frac{\partial S_i(z_i, z_{i+1})}{\partial z_{i+1}}$ are both $\mathcal{C}^1$ functions on $\mathbb{R}$, and exhibit homogeneous in the bilimit.

In (27), we have $W(z) = 0$ when $z = 0$. Then, we will prove that $W(z) < 0$ while $z \neq 0$. Consider the hypersurfaces as

$$\mathcal{Z}_1 = \{\varphi_1(z_1) = z_2\}$$
$$\mathcal{Z}_2 = \mathcal{Z}_1 \cap \{\varphi_2(z_2) = z_3\}$$

with $\mathcal{Z}_2 \subset \mathcal{Z}_1 \subset \mathbb{R}^n$.

Denote the values of W on the hypersurfaces $\mathcal{Z}_1$and$\mathcal{Z}_2$ as $W_{\mathcal{Z}_1}$ and $W_{\mathcal{Z}_2}$, respectively, and we have

$$W_{\mathcal{Z}_1}(z_2, z_3) = -\tilde{k}_2\vartheta_2(z_2, z_3)\left[\varphi_2(z_2) - z_3\right] - \tilde{k}_3(s_2 + \vartheta_3)\left[\varphi_3 \circ \varphi_2(z_2) - \frac{M}{k_3}[-1, 1]\right] \tag{28}$$

$$W_{\mathcal{Z}_2}(z_3) = -\tilde{k}_3\left(\beta_{0,3}{z_3}^{p_0-1} + \beta_{\infty,3}{z_3}^{p_\infty-1}\right) \times \left(\kappa_3{z_3}^{1+d_0} + \theta_3{z_3}^{1+d_\infty} - \frac{M}{k_3}[-1, 1]\right). \tag{29}$$

As mentioned in (20), $d_0 = -1$, and κ_3 and k_3 are positive parameters. By selecting κ_3 and k_3, $\tilde{M} = \frac{M}{\kappa_3 k_3} < 1$ can be guaranteed. Then, we have $\kappa_3(z_3^0 - \tilde{M}[-1, 1]) = \kappa_n z_n^0\left[1 - \tilde{M}, 1 + \tilde{M}\right]$. Substituting this condition into (29), we can derive the following inequality:

$$W_{\mathcal{Z}_2}(z_3) \leqslant W^*_{\mathcal{Z}_2}(z_3) = -\tilde{k}_3\left(\beta_{0,3}z_3^{p_0-1} + \beta_{\infty,3}z_3^{p_\infty-1}\right) \times \left[\kappa_3(1 - \tilde{M}) + \theta_3|z_3|^{1+d_\infty}\right]. \tag{30}$$

Based on (30), it can be observed that $W^*_{\mathcal{Z}_2}(z_3)$ is single-valued, u.s.c., homogeneous in the bilimit, and negative definite for any $\tilde{k}_3 > 0$. By applying Lemma 1, we can conclude the existence of $\tilde{k}_1 > 0$, $\tilde{k}_2 > 0$, and $\tilde{k}_3 > 0$ such that $W < 0$ and $\dot{V} < 0$.

Consider the u.s.c. functions $\zeta(z) = -\dot{V}$ and $\phi(z) = \alpha_0 V^{\frac{p_0+d_0}{p_0}} + \alpha_\infty V^{\frac{p_\infty+d_\infty}{p_\infty}}$, where α_0 and α_∞ are positive scalars. As $\zeta > 0$ for $z \neq 0$, the conditions in Lemma 2 are satisfied. Hence, there exists a positive scalar λ such that $\phi(x) \leqslant \lambda\zeta(z)$, which can be expressed as

$$\dot{V} \leqslant -\eta_0 V^{\frac{p_0+d_0}{p_0}} - \eta_\infty V^{\frac{p_\infty+d_\infty}{p_\infty}} \tag{31}$$

where η_0 and η_∞ are positive scalars. Based on the fixed-time convergence principal [30], the estimate errors will converge to zero within a fixed time estimated by (21). Thus, this completes the proof. ■

Remark 3: Equation (18) represents a set of composite functions derived from (19) with the powers in (20). It is important to note that, based on the proposed construction, (18) exhibits homogeneous in the bilimit [26], [30]. Consequently, the differentiators derived from (18) also demonstrate homogeneous in the bilimit. By leveraging this characteristic for the differentiators, we can deduce the proof for fixed-time convergence of the estimate errors of the designed differentiators based on the results presented in Lemmas 1 and 2.

B. Controller Design

To construct the model-free control protocol, the preview error model (5) can be reorganized by selecting a positive constant gain $\bar{b}$ with the proposed differentiator as follows:

$$H(t) + \bar{b}\ddot{\hat{\sigma}}(t) - \delta_{\mathrm{f}}(t) = 0 \tag{32}$$

with $H(t) = -b^{-1}h(t) + (b^{-1} - \bar{b})\ddot{\sigma}(t) + \bar{b}(\ddot{\sigma} - \ddot{\hat{\sigma}})$.

In (32), $H(t)$ consists of multiple components, namely, the vehicle dynamics item $h(t)$, the input gain b incorporating vehicle parameters, the preview error dynamics $\ddot{\sigma}$, and the estimate error of $\ddot{\hat{\sigma}}$. As a result of the presence of these specific components, directly obtaining the precise information or expression of $H(t)$ becomes challenging.

To achieve the model-free feature, we can estimate H by utilizing the TDE approach, which is defined by

$$\hat{H}(t) = H(t - t_\lambda) = \delta_{\mathrm{f}}(t - t_\lambda) - \bar{b}\ddot{\hat{\sigma}}(t - t_\lambda) \tag{33}$$

where t_λ represents a small delay time; $\hat{H}(t)$ represents the estimation of H using TDE. For brevity, we omit (t) in variables without any delay. In order to ensure the boundedness of the TDE error, the constant gain $\bar{b}$ plays a crucial role. It has been proved that the TDE error can be bounded by satisfying the inequality $|1 - b\bar{b}| < 1$ [31]. Therefore, the TDE error $\varepsilon = \hat{H} - H$ can be bounded by an unknown positive constant d_ε such that $|\varepsilon| \leqslant d_\varepsilon$.

Then, we present the following theorem and illustrate the control structure of FTPPC-MF in Fig. 1.

Theorem 2: Consider the FTPPC-MF protocol:

$$\delta_{\mathrm{f}} = -\hat{b}\left(\delta_{\mathrm{f1}} + \delta_{\mathrm{f2}}\right) + \hat{H} - \hat{d}_\varepsilon\,\mathrm{sign}(\omega) \tag{34}$$

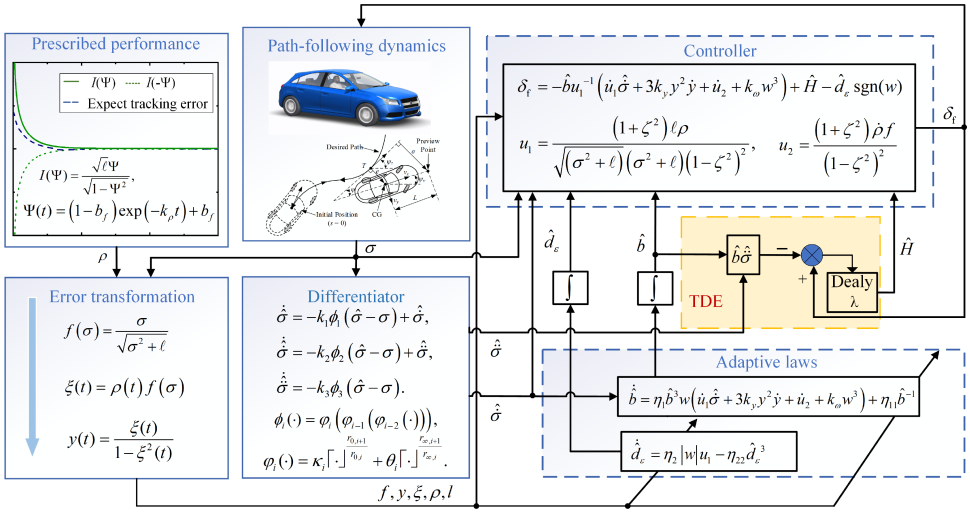

Fig. 1. Block diagram of FTPPC-MF.

with

$$\delta_{f1} = u_1{}^{-1}\left(\dot{u}_1\hat{\sigma} + 3k_y y^2\dot{y} + \dot{u}_2\right)$$
$$\delta_{f2} = u_1{}^{-1}k_\omega w^3 \tag{35}$$

updated by

$$\dot{\hat{b}} = \eta_1\hat{b}^3 w\left(\dot{u}_1\hat{\sigma} + 3k_y y^2\dot{y} + \dot{u}_2 + k_\omega w^3\right) + \eta_{11}\hat{b}^{-1}$$
$$\dot{\hat{d}}_\varepsilon = \eta_2\left|w\right|u_1 - \eta_{22}\hat{d}_\varepsilon^3 \tag{36}$$

where ω, u_1, and u_2 are defined in (40); k_y and k_ω are positive control gains; η_1, η_2, η_{11}, and η_{22} are positive parameters to update the adaptive laws; $\dot{u}_1$, $\dot{u}_2$, and $\dot{y}$ represent the time derivatives of u_1, u_2, and y, respectively. $\dot{u}_1$, $\dot{u}_2$, and $\dot{y}$ are straightforward to calculate, and their detailed expressions are omitted for brevity. Then, the proposed control objective, which combines the fixed-time convergence and the prescribed performance (6), can be achieved for the preview error.

Proof: To ensure the fulfillment of the prescribed performance, an error transformation is applied to the preview error, given by

$$f(\sigma) = \frac{\sigma}{\sqrt{\sigma^2 + \ell}} \tag{37}$$

where $\ell = 1 - k_\infty^2$.

From (37), it can be observe that if there exists a positive constant $\bar{f}$ satisfying $|f(\sigma)| \leqslant \bar{f} < 1$, then $\sigma = \frac{f\sqrt{\ell}}{\sqrt{1-f^2}}$ remains bounded.

In addition, a barrier function is introduced as follows:

$$y(t) = \frac{\xi(t)}{1 - \xi^2(t)} \tag{38}$$

where $\xi(t) = \rho(t)f(\sigma)$, and $\rho(t) = \frac{1}{\psi(t)}$. Then, by ensuring that y remains uniformly and ultimately bounded, we can guarantee that $|\xi(t)| = |\rho(t)f(\sigma)| < 1$, and the satisfaction of the preset constraints (6) for the preview error throughout the entire path-following process.

A Lyapunov function candidate is selected as follows:

$$V_1 = \frac{1}{2}y^2. \tag{39}$$

The time derivative of (39) is calculated as

$$\begin{aligned}\dot{V}_1 = y\Bigg(&-k_y y^3 + \underbrace{\frac{\left(1+\xi^2\right)\ell\rho}{\left(1-\xi^2\right)^2\sqrt{\left(\sigma^2+\ell\right)\left(\sigma^2+\ell\right)}}}_{u_1}\dot{\sigma} \\ &+ \underbrace{\left(1+\xi^2\right)\dot{\rho}f\left(1-\xi^2\right)^{-2}}_{u_2} + k_y y^3\Bigg) \\ &= y(-k_y y^3 + u_1\dot{\sigma} + u_2 + k_y y^3)\end{aligned} \tag{40}$$

which implies that y can be driven to zero within a fixed time if $\omega = u_1\dot{\sigma} + u_2 + k_y y^3 = 0$ is satisfied. Recalling Theorem 1, it is known that the estimate errors based on the proposed differentiators will be stabilized after a small fixed time t_d. Therefore, for $t \geqslant t_d$, we can redefine the following Lyapunov function:

$$V_2 = \frac{1}{2}y^2 + \frac{1}{2}w^2 + \frac{1}{2\eta_1}\tilde{b}^2 + \frac{1}{2\eta_2\bar{b}}\tilde{d}_\varepsilon^2 \tag{41}$$

where $\tilde{b} = \hat{b}^{-1} - \bar{b}^{-1}$, and $\tilde{d}_\varepsilon = \hat{d}_\varepsilon - d_\varepsilon$.

Differentiating (41) and applying controller (34) produce

$$\begin{aligned}\dot{V}_2 &= y\dot{y} + w\dot{w} - \eta_1{}^{-1}\tilde{b}^{-2}\dot{\hat{b}} + \bar{b}^{-1}\eta_2{}^{-1}\dot{\hat{d}}_\varepsilon\tilde{d}_\varepsilon \\ &= -k_y y^4 + w\left(\dot{u}_1\dot{\sigma} + u_1\ddot{\sigma} + \dot{u}_2 + 3k_y y^2\dot{y}\right) \\ &\quad - \eta_1{}^{-1}\tilde{b}\hat{b}^{-2}\dot{\hat{b}}^2 + \bar{b}^{-1}\eta_2{}^{-1}\dot{\hat{d}}_\varepsilon\tilde{d}_\varepsilon \\ &= -k_y y^4 + w\Big[\dot{u}_1\dot{\sigma} + u_1\left(\bar{b}^{-1}\delta_f - \bar{b}^{-1}H\right) \\ &\quad + \dot{u}_2 + 3k_y y^2\dot{y}\Big] - \eta_1{}^{-1}\tilde{b}^{-2}\dot{\hat{b}} + \bar{b}^{-1}\eta_2{}^{-1}\dot{\hat{d}}_\varepsilon\tilde{d}_\varepsilon\end{aligned}$$

$$
\begin{aligned}
&= -k_y y^4 - \bar{b}^{-1}\hat{b}k_\omega w^4 + u_1\bar{b}^{-1}w\left[d_\varepsilon - \hat{d}_\varepsilon\,\mathrm{sgn}(w)\right] \\
&\quad + w\Big(\dot{u}_1\dot{\sigma} - \bar{b}^{-1}\hat{b}\dot{u}_1\hat{\sigma} + 3k_y y^2\dot{y} - \bar{b}^{-1}\hat{b}3k_y y^2\dot{y} \\
&\quad + \dot{u}_2 - \bar{b}^{-1}\hat{b}\dot{u}_2\Big) - \eta_1^{-1}\hat{b}^{-2}\hat{b} + \bar{b}^{-1}{\eta_2}^{-1}\dot{\hat{d}}_\varepsilon\tilde{d}_\varepsilon. \qquad (42)
\end{aligned}
$$

By invoking Lemmas 3 and 4, and substituting (36) into (42), we can obtain that

$$
\begin{aligned}
\dot{V}_2 \le\ & -k_y y^4 - k_\omega w^4 + {\eta_1}^{-1}\eta_{11}\left(-k_b\tilde{b}^4 + k_{bb}b^4\right) \\
& + \bar{b}^{-1}{\eta_2}^{-1}\eta_{22}\left(-k_\varepsilon\tilde{d}_\varepsilon^4 + k_{\varepsilon\varepsilon}{d_\varepsilon}^4\right) \\
\le\ & -\frac{1}{2}\Big(k_y y^4 + k_\omega w^4 + {\eta_1}^{-1}\eta_{11}k_b\tilde{b}^4 \\
& + \bar{b}^{-1}{\eta_2}^{-1}\eta_{22}k_\varepsilon\tilde{d}_\varepsilon^4\Big) - \frac{1}{4}\Big(k_y y^{2q} + k_\omega w^{2q} \\
& + {\eta_1}^{-1}\eta_{11}k_b\tilde{b}^{2q} + \bar{b}^{-1}{\eta_2}^{-1}\eta_{22}k_\varepsilon\tilde{d}_\varepsilon^{2q}\Big) \\
& + {\eta_1}^{-1}\eta_{11}k_{bb}b^4 + \bar{b}^{-1}{\eta_2}^{-1}\eta_{22}k_{\varepsilon\varepsilon}{d_\varepsilon}^4 \\
& + \frac{1}{2}\Big(k_y + k_\omega + {\eta_1}^{-1}\eta_{11}k_b \\
& + \bar{b}^{-1}{\eta_2}^{-1}\eta_{22}k_\varepsilon\Big) \\
\le\ & -\lambda_1 V^2 - \lambda_2 V^q + C \qquad (43)
\end{aligned}
$$

where $0 < q < 1$, and the parameters are given as follows:

$$
\begin{aligned}
\lambda_1 &= 2^{-1}\min\left\{k_y, k_\omega, {\eta_1}^{-1}\eta_{11}k_b, \left(\bar{b}\eta_2\right)^{-1}\eta_{22}k_\varepsilon\right\} \\
\lambda_2 &= \frac{2^q}{4}\min\left\{k_y, k_\omega, {\eta_1}^{q-1}\eta_{11}k_b, \left(\bar{b}\eta_2\right)^{q-1}\eta_{22}k_\varepsilon\right\} \\
C &= {\eta_1}^{-1}\eta_{11}k_{bb}b^4 + \left(\bar{b}\eta_2\right)^{-1}\eta_{22}k_{\varepsilon\varepsilon}{d_\varepsilon}^4 \\
&\quad + \frac{1}{2}\left(k_y + k_\omega + {\eta_1}^{-1}\eta_{11}k_b + \left(\bar{b}\eta_2\right)^{-1}\eta_{22}k_\varepsilon\right). \qquad (44)
\end{aligned}
$$

Resorting to Lemma 5, y is bounded by y_m given as

$$
y_m = \min\left\{\left[\frac{4\,C}{\lambda_1\,(1-\omega_2)}\right]^{\frac{1}{4}}, \left[\frac{2^q C}{\lambda_2\,(1-\omega_2)}\right]^{\frac{1}{2q}}\right\} \qquad (45)
$$

with $0 < \omega_2 < 1$.

Then, σ is driven toward a residual set of (6) as follows:

$$
|\sigma| \leqslant \sqrt{\frac{\ell z^2}{\rho^2 - z^2}} \qquad (46)
$$

where $z = \sqrt{1 + \frac{1}{4y_m{}^2}} - \frac{1}{2y_m}$.

The fixed settling time t_c is estimated and bounded by

$$
t_c \leqslant T_{\max} = (\lambda_1\omega_2)^{-1} + [\lambda_2\omega_2(1-q)]^{-1}. \qquad (47)
$$

By considering the fixed settling time of the differentiators, the total settling time can be calculated by $t_c + t_d$.

TABLE I
VEHICLE PARAMETERS IN SIMULATION

Vehicle parameter	Value
m	1230 kg
l_f	1.04 m
l_r	1.56 m
I_z	1343 kg·m^2
c_f	96300 N/rad
c_r	64200 N/rad

To demonstrate the satisfaction of the prescribed performance constraints (6) throughout the entire path-following process, the following results are presented.

From (43), we have

$$
\begin{cases}
\dot{V}_2 \leqslant -\lambda_1 V_2^2 + C \leqslant -\lambda_1 V_2 + C, & 1 \leqslant V_2 \\
\dot{V}_2 \leqslant -\lambda_2 V_2^q + C \leqslant -\lambda_2 V_2 + C, & 0 \leqslant V_2 < 1
\end{cases} \qquad (48)
$$

which implies that

$$
\dot{V}_2 \leqslant -\min(\lambda_1, \lambda_2)V_2 + C. \qquad (49)
$$

Then, we have

$$
\begin{aligned}
V_2 \leqslant\ & \left(V_2(0) - \frac{C}{\sqrt{\min(\lambda_1, \lambda_2)}}\right)\exp(-\min(\lambda_1, \lambda_2)t) \\
& + \frac{C}{\min(\lambda_1, \lambda_2)}. \qquad (50)
\end{aligned}
$$

By observing that $y \le \sqrt{2V_2}$, we can ensure the uniform and ultimate boundedness of y by continuously decreasing V_2. Thus, the prescribed performance is consistently achieved. This completes the proof. ■

Remark 4: The prescribed performance constraints defined in (6) imposes limitations on the convergence behavior of the preview error, controlled by the boundary parameters k_ρ and k_∞. To achieve rapid convergence in vehicle path following, it is desirable to choose a large k_ρ and a small k_∞. However, during simulation and experiment studies, we have observed that the practical vehicle cannot always accommodate arbitrary small prescribed performance boundaries. This limitation can potentially lead to system instabilities, considering the limited capabilities of the actual vehicle system.

IV. SIMULATION STUDIES

To validate the effectiveness of the proposed FTPPC-MF protocol, we conduct simulations using the CarSim platform, which incorporates nonlinear vehicle dynamics with uncertainties and disturbances. The simulated scenario involves controlling an AGV to follow an S-curve path at a speed of $v = 60$ km/h. Table I provides the relevant parameters in the simulations. Furthermore, we implement a comparative path-following controller based on the conventional TDC model-free scheme, which does

TABLE II
PARAMETERS FOR CONTROLLER AND DIFFERENTIATOR

Controller	Value
FTPPC-MF	$k_y = 0.4,, k_\omega = 2,\ k_{sat} = 2,$ $\eta_1 = 10^{-7}, \eta_{11} = 10^{-9}, \eta_2 = 10^{-14}, \eta_{22} = 10^{-14}.$
Conventional TDC	$\bar{b} = 0.00009,\ K_D = 3,\ K_P = 3.$
Differentiator	$k_1 = 3,\ k_2 = 1.5\sqrt{3},\ k_3 = 5.1,$ $\kappa_1 = 5,\ \kappa_2 = 5,\ \kappa_3 = 5,$ $\theta_1 = 5,\ \theta_2 = 10,\ \theta_3 = 5.$

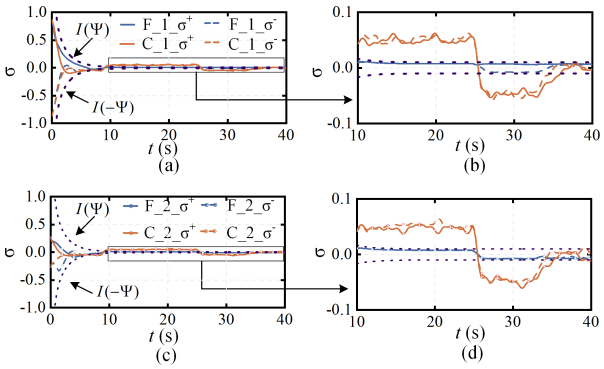

Fig. 2. Simulation results. (a), (b) $\sigma(0) = \pm 0.868$. (c), (d) $\sigma(0) = \pm 0.268$.

not incorporate the prescribed performance and fixed-time convergence features as follows:

$$\delta_{\mathrm{f}} = -\bar{b}\left(K_D\hat{\sigma} + K_P\sigma\right) + \hat{H} \tag{51}$$

where K_D and K_P are positive control gains.

To ensure a fair comparison, the comparative controllers utilize the same differentiators. Specifically, the initial value of parameter $\hat{b}$ in the FTPPC-MF controller is set to the same value as the $\bar{b}$ parameter in the conventional TDC controller. This ensures consistency and allows for a meaningful evaluation of the performance of both controllers. The specific parameters used for the controllers and differentiators in the simulations can be found in Table II. The constraint function in (8) is preset as follows:

$$\Psi(t) = (1 - 0.01)\exp(-0.5t) + 0.01. \tag{52}$$

The controlled vehicle is initially positioned with various preview errors, specifically, $\sigma(0) = \pm 0.868$ m (1_σ^+ and 1_σ^-) incorporating $e(0) = \pm 0.9$ m and $\psi(0) = \pm 0.02$ rad, and $\sigma(0) = \pm 0.268$ m (2_σ^+ and 2_σ^-) incorporating $e(0) = \pm 0.3$m and $\psi(0) = \pm 0.02$ rad.

The simulation result is plotted in Fig. 2, which shows that both the FTPPC-MF (abbreviated by "F" in the figures) and conventional TDC (abbreviated by "C" in the figures) protocols are able to stabilize the preview errors. Notably, the FTPPC-MF protocol consistently ensures that σ remains within the preset constraints. Regardless of the change in initial conditions, the

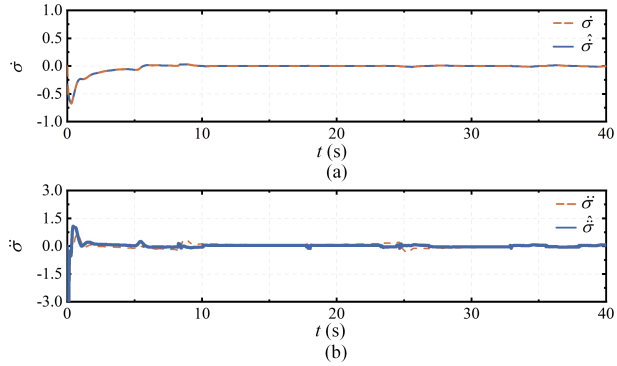

Fig. 3. Results for differentiators. (a) First-order dynamics of preview error. (b) Second-order dynamics of preview error.

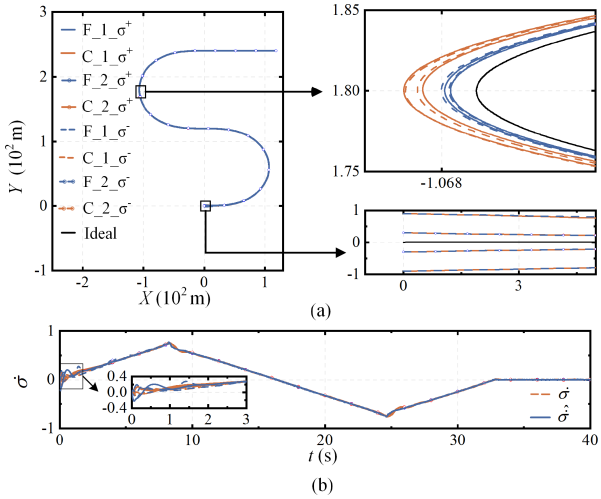

Fig. 4. Trajectories and steering inputs for all cases. (a) Trajectories. (b) Steering inputs.

FTPPC-MF protocol maintains satisfactory path-following performance within the prescribed range. On the other hand, the vehicle controlled by the conventional TDC protocol fails to keep the preview error within a small neighborhood of zero, leading to violations of the preset boundaries in (52), as depicted in Fig. 2(b) and (d). In Fig. 3, we provide the results of the proposed differentiators specifically for the $F\_1\_\sigma^+$ case for brevity. It can be observed that the proposed differentiators accurately estimate the high-order dynamics of the preview error. Fig. 4 shows the vehicle trajectories and steering inputs for all cases. From the simulation comparison of the vehicle trajectories, it is evident that the designed FTPPC-MF protocol consistently outperforms the conventional TDC protocol in terms of both transient and steady-state behaviors. Finally, the control objectives proposed in Section II have been successfully achieved based on the simulation results.

V. EXPERIMENT STUDIES

To further demonstrate the performance of the FTPPC-MF protocol, practical vehicle experiments are conducted using a scaled vehicle with the parameters listed in Table III. As shown in Fig. 5, the vehicle system is equipped with an onboard

TABLE III
PARAMETERS FOR PRACTICAL-SCALED VEHICLE

Parameter	Value
m	35.16 kg
l_{f}	0.25 m
l_{r}	0.25 m
I_z	2.188 kg·m^2
c_{f}	1130 N/rad
c_{r}	1130 N/rad

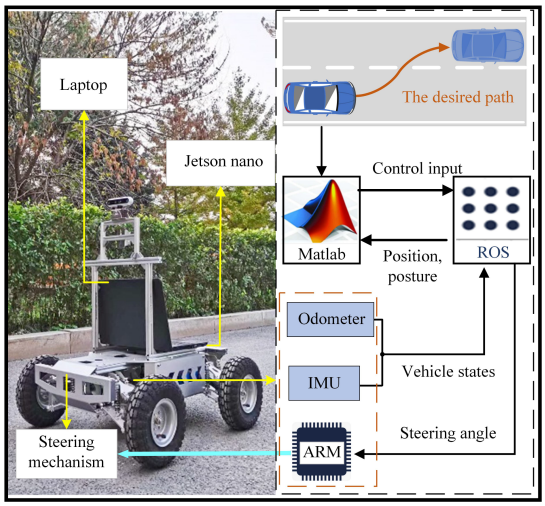

Fig. 5. Experiment platform and schematic diagram.

TABLE IV
PARAMETERS FOR CONTROLLER AND DIFFERENTIATOR

Controller	Value
FTPPC-MF	$\hat{b}(0) = 1.785 * 10^{-5},\ k_y = 0.001,$ $k_\omega = 4500,\ k_{sat} = 1,$ $\eta_1 = 10^{-14}, \eta_{11} = 10^{-14},$ $\eta_2 = 10^{-13}, \eta_{22} = 10^{-13}.$
Conventional TDC	$\bar{b} = 0.0009,\ K_D = 20,\ K_P = 3.$
Differentiator	$k_1 = 3,\ k_2 = 1.5\sqrt{3},\ k_3 = 5.1,$ $\kappa_1 = 5,\ \kappa_2 = 5,\ \kappa_3 = 5,$ $\theta_1 = 5,\ \theta_2 = 10,\ \theta_3 = 5.$

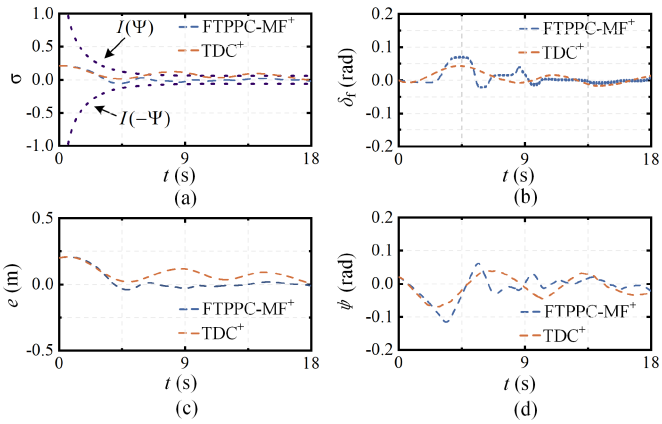

Fig. 6. Experimental results for $\sigma(0) = 0.2114$. (a) Preview errors. (b) Steering angles. (c) Distance offsets. (d) Bearing angle offsets.

laptop (AMD Ryzen 9 5900HX, 32 GB RAM) to implement the proposed control protocol. The vehicle's location and posture are obtained by fusing the information from the encoders and the inertial measurement unit (IMU, MPU6050) collected by the Cortex ARM STM32 F103RCT6. In terms of fusion accuracy, we evaluate the performance of the sensors fused by IMU and odometer during the vehicle's path-following period in the experiments. The achieved results indicate an error of 0.26 per 100 m traveled, a yaw rate accuracy of 0.5°/s, and a heading accuracy of 1°. It is important to note that these accuracy values are influenced by time and can accumulate errors. However, given the relatively short duration of the path following in the context of this article, the accumulated errors are considered negligible. The preview error is then transmitted to the proposed control protocol running on the laptop, and the calculated steering input is fed back to the chassis system to execute the desired vehicle motion. Real-time data transformation between the laptop and the chassis system is facilitated by robot operating system (ROS) running on the Jetson Nano. During the experiment implementation, a time step of 10 ms is set, and the AGV is controlled to perform a lane change maneuver with a velocity of $v = 1$ m/s. The parameters for the FTPPC-MF and conventional TDC controllers are selected, as listed in Table IV. The constraint function is preset as

$$\Psi(t) = (1 - 0.06)\exp(-0.6t) + 0.06. \tag{53}$$

To demonstrate the robustness of the FTPPC-MF protocol, various initial preview errors are considered, including different lateral distance and bearing angle offsets. Specifically, for positive initial preview error with $\sigma(0) = 0.21$ m incorporating $e(0) = 0.2$ m and $\psi(0) = 0.02$ rad, the preview error is effectively stabilized to a small neighborhood of zero using the FTPPC-MF protocol, as depicted in Fig. 6. Throughout the entire lane-change maneuver operation, the preview error remains within the preset boundaries. However, when employing the conventional TDC controller, the preset constraints are violated by the preview error.

Similarly, for negative initial preview error with $\sigma(0) = -0.33$ m incorporating $e(0) = -0.36$ m and $\psi(0) = 0.05$ rad, the vehicle controlled by the proposed FTPPC-MF protocol maintains the preview error within the preset constraints, as shown in Fig. 7. In contrast, although the conventional TDC controller ultimately stabilizes the preview error to a small neighborhood of zero, the preview error surpassed the preset boundaries between 3 and 10 s. The trajectories of vehicle for all cases are shown in Fig. 8.

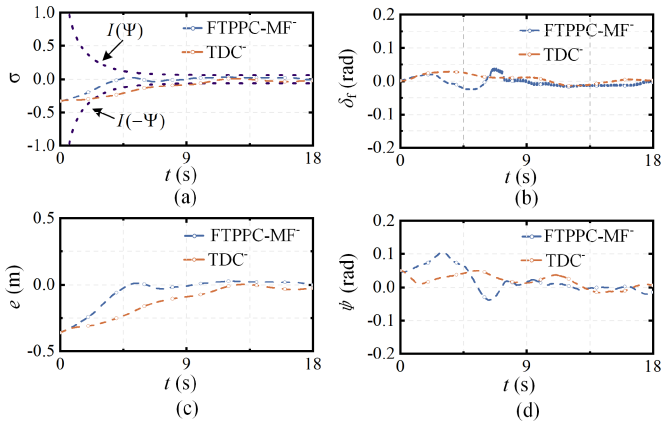

Fig. 7. Experimental results for $\sigma(0) = -0.3315$. (a) Preview errors. (b) Steering angles. (c) Distance offsets. (d) Bearing angle offsets.

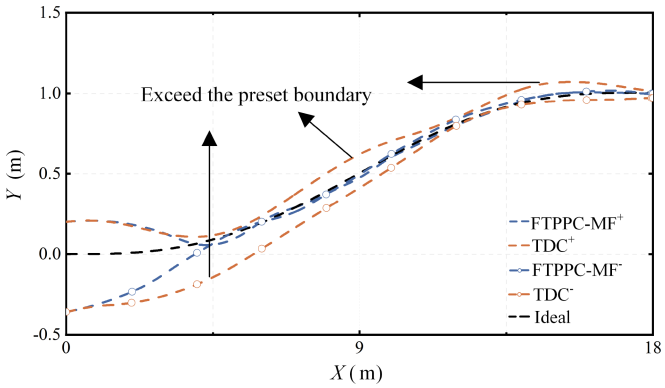

Fig. 8. Trajectories for all cases.

To sum up, both the proposed FTPPC-MF protocol and the conventional TDC scheme can achieve the path-following control objective. However, the FTPPC-MF protocol consistently outperforms the conventional TDC scheme in terms of both transient-state and steady-state performances. The fixed-time scheme employed in the FTPPC-MF protocol ensure a fast convergence rate for the controlled system, while the PPC scheme guarantees that the preview error satisfies the preset constraint condition. By integrating the fixed-time and PPC protocols, the FTPPC-MF protocol achieves superior path-following performance. In addition, the use of the TDE allows for the fusion of model-free properties. Even though a large boundary selection may lead to comparable results with the conventional TDC scheme, it is crucial to emphasize that the control performance of the FTPPC-MF protocol is guided by prior knowledge derived from the PPC-based scheme. This aspect holds significant importance in practical applications.

VI. Conclusion

In conclusion, we have developed a novel FTPPC-MF protocol for autonomous vehicle systems to effectively follow desired paths. The FTPPC-MF controller possesses a model-free characteristic, as it does not require any knowledge or parameters of the controlled vehicle. By integrating a prescribed performance function with a fixed-time control scheme, the FTPPC-MF protocol ensures robust convergence of the preview error, regardless of initial conditions, while adhering to preset boundaries. Through simulation and experimental studies, we have demonstrated that the proposed FTPPC-MF protocol successfully achieves the control objective and consistently outperforms the conventional TDC scheme.

Appendix

In order to apply the proposed technique in vehicle longitudinal speed control, it is necessary to consider the longitudinal vehicle dynamics, which can be described as follows: [24]

$$\dot{v}_x = \frac{1}{mR}T_a + \beta\gamma v_x - \frac{1}{m}F_{\text{fay}}\sin\delta_{\text{f}} + \frac{\cos\delta_{\text{f}} - 1}{m}F_{\text{fax}} - \frac{1}{mR}\sum_{4}^{i=1}\Delta T_i. \tag{54}$$

The longitudinal speed error is denoted by $e_v = v_x - v_{\text{d}}$. Taking the time derivative of e_v yields

$$\begin{aligned}\dot{e}_v &= \frac{1}{mR}T_{\text{a}} + \beta\gamma v_x - \frac{1}{m}F_{\text{fay}}\sin\delta_{\text{f}} + \frac{\cos\delta_{\text{f}} - 1}{m}F_{\text{fax}} \\ &\quad - \frac{1}{mR}\sum_{4}^{i=1}\Delta T_i - \dot{v}_{\text{d}} \\ &= b_v T_{\text{a}} + h_v\end{aligned} \tag{55}$$

where $b_v = \frac{1}{mR}$, and $h_v = \beta\gamma v_x - \frac{1}{m}F_{\text{fay}}\sin\delta_{\text{f}} + \frac{\cos\delta_{\text{f}}-1}{m}F_{\text{fax}} - \frac{1}{mR}\sum_{4}^{i=1}\Delta T_i - \dot{v}_{\text{d}}$.

To estimate the longitudinal speed error dynamics and construct the model-free control protocol, a positive constant gain $\bar{b}_v$ is introduced, and the error dynamics in (55) are then reorganized as follows:

$$H_v(t) + \bar{b}_v\dot{e}_v(t) - T_{\text{a}}(t) = 0 \tag{56}$$

with $H_v(t) = -b_v^{-1}h_v + (b_v^{-1} - \bar{b}_v)\dot{e}_v$.

Based on (56), the TDE approach can be employed to estimate $H_v(t)$ as follows:

$$\hat{H}_v(t) = T_{\text{a}}(t - t_\lambda) - \bar{b}_v\dot{e}_v(t - t_\lambda). \tag{57}$$

Similar to (6)–(8), we employ the prescribed performance boundary functions $I(-\Psi_v)$ and $I(\Psi_v)$ with Ψ_v, $k_{\infty v}$, and $k_{\rho v}$ for e_v. Then, an error transformation for e_v can be given by

$$f_v(e_v) = \frac{e_v}{\sqrt{e_v^2 + \ell_v}} \tag{58}$$

and a barrier function is introduced as follows:

$$y_v(t) = \frac{\xi_v(t)}{1 - \xi_v^2(t)} \tag{59}$$

where $\xi_v(t) = \rho_v(t)f(e_v)$, $\rho_v(t) = \frac{1}{\Psi_v(t)}$, and $\ell_v = 1 - k_{\infty v}^2$.

In (57), we can observe that the longitudinal acceleration required by the TDC-based algorithm can be easily obtained from the IMU, eliminating the necessity for a differentiator. Based on a similar proof as in Theorem 2, the fixed-time PPC

model-free control protocol for the longitudinal vehicle speed is constructed as follows:

$$\begin{cases} T_{\mathrm{a}} = -\hat{b}_v u_{v1}^{-1}\left(u_{v2} + k_{v1} y_v^3\right) + \hat{H}_v - \hat{d}_{v\varepsilon}\,\mathrm{sign}\left(y_v\right) \\ u_{v1} = \dfrac{\left(1+\xi_v^2\right)\ell_v \rho_v}{\left(1-\xi_v^2\right)^2\sqrt{\left(e_v^2+\ell\right)}\left(e_v^2+\ell_v\right)} \\ u_{v2} = \dfrac{\left(1+\xi_v^2\right)\dot{\rho}_v f_v}{\left(1-\xi_v^2\right)^2} \end{cases} \tag{60}$$

updated by

$$\begin{cases} \dot{\hat{b}}_v = \eta_{v1}\hat{b}_v^3 y_v\left(u_{v2} + k_{v1} y_v{}^3\right) + \eta_{v11}\hat{b}_v^{-1} \\ \dot{\hat{d}}_{v\varepsilon} = \eta_{v2}\left|y_v\right| u_{v1} - \eta_{v22}\hat{d}_{v\varepsilon}{}^3 \end{cases} \tag{61}$$

where k_{v1} is a positive control gain; $\eta_{v1}, \eta_{v11}, \eta_{v2}$, and η_{v22} are positive gains for adaptive laws.

REFERENCES

[1] C. Huang, C. Lv, P. Hang, and Y. Xing, "Toward safe and personalized autonomous driving: Decision-making and motion control with DPF and CDT techniques," *IEEE/ASME Trans. Mechatron.*, vol. 26, no. 2, pp. 611–620, Apr. 2021.

[2] T. Faulwasser and R. Findeisen, "Nonlinear model predictive control for constrained output path following," *IEEE Trans. Autom. Control*, vol. 61, no. 4, pp. 1026–1039, Apr. 2016.

[3] Z. Wang, X. Zhou, and J. Wang, "Extremum-seeking-based adaptive model-free control and its application to automated vehicle path tracking," *IEEE/ASME Trans. Mechatron.*, vol. 23, no. 4, pp. 3874–3884, Oct. 2022.

[4] M. W. Mehrez, K. Worthmann, G. K. Mann, R. G. Gosine, and T. Faulwasser, "Predictive path following of mobile robots without terminal stabilizing constraints," *IFAC-PapersOnLine*, vol. 50, no. 1, pp. 9852–9857, Jul. 2017.

[5] Y. Huang, F. Wang, A. Li, Y. Shi, and Y. Chen, "Development and performance enhancement of an overactuated autonomous ground vehicle," *IEEE/ASME Trans. Mechatron.*, vol. 26, no. 1, pp. 33–44, Feb. 2021.

[6] R. Wang, H. Jing, C. Hu, F. Yan, and N. Chen, "Robust H_∞ path following control for autonomous ground vehicles with delay and data dropout," *IEEE Trans. Intell. Transp. Syst.*, vol. 17, no. 7, pp. 2042–2050, Jul. 2016.

[7] C. Hu, R. Wang, and F. Yan, "Integral sliding mode-based composite nonlinear feedback control for path following of four-wheel independently actuated autonomous vehicles," *IEEE Trans. Transp. Electrific.*, vol. 2, no. 2, pp. 221–230, Jun. 2016.

[8] C. Hu et al., "MME-EKF-Based path-tracking control of autonomous vehicles considering input saturation," *IEEE Trans. Veh. Technol.*, vol. 68, no. 6, pp. 5246–5259, Jun. 2019.

[9] X. Han, I. Kkdemiral, and M. S. Erden, "Time delay control with sliding mode observer for a. class of nonlinear systems: Performance and stability," *Int. J. Robust Nonlinear Control*, vol. 31, no. 18, pp. 9231–9252, Sep. 2021.

[10] Y. Wang, L. Liu, D. Wang, F. Ju, and B. Chen, "Time-delay control using a novel nonlinear adaptive law for accurate trajectory tracking of cable-driven robots," *IEEE Trans. Ind. Informat.*, vol. 16, no. 8, pp. 5234–5243, Aug. 2020.

[11] Z. Liang, Z. Wang, J. Zhao, and X. Ma, "Fast finite-time path-following control for autonomous vehicle via complete model-free approach," *IEEE Trans. Ind. Informat.*, vol. 19, no. 3, pp. 2838–2846, Mar. 2023.

[12] S. Baek, J. Baek, W. Kwon, and S. Han, "An adaptive model uncertainty estimator using delayed state-based model-free control and its application to robot manipulators," *IEEE/ASME Trans. Mechatron.*, vol. 27, no. 6, pp. 4573–4584, Dec. 2022.

[13] S. Roy, I. N. Kar, J. Lee, and M. Jin, "Adaptive-robust time-delay control for a class of uncertain Euler–Lagrange systems," *IEEE Trans. Ind. Inform.*, vol. 64, no. 9, pp. 7109–7119, Sep. 2017.

[14] C. Hu and J. Wang, "Trust-based and individualizable adaptive cruise control using control barrier function approach with prescribed performance," *IEEE Trans. Intell. Transp. Syst.*, vol. 23, no. 7, pp. 6974–6984, Jul. 2022.

[15] C. Hu et al., "RISE-Based integrated motion control of autonomous ground vehicles with asymptotic prescribed performance," *IEEE Trans. Syst. Man Cybern.: Syst.*, vol. 51, no. 9, pp. 5336–5348, Sep. 2021.

[16] Z. Liang, Z. Wang, J. Zhao, P. K. Wong, Z. Yang, and Z. Ding, "Fixed-time and fault-tolerant path-following control for autonomous vehicles with unknown parameters subject to prescribed performance," *IEEE Trans. Syst. Man Cybern.: Syst.*, vol. 53, no. 4, pp. 2363–2373, Apr. 2023.

[17] X. Zhang, Y. Wang, Z. Yang, J. Huang, and Y. Su, "Path tracking control for autonomous vehicles with saturated input: A fuzzy fixed–time learning control approach," *IET Intell. Transp. Syst.*, vol. 16, no. 4, pp. 531–542, Jan. 2022.

[18] X. Jin, S. -L. Dai, and J. Liang, "Fixed-time path-following control of an autonomous vehicle with path-dependent performance and feasibility constraints," *IEEE Trans. Intell. Veh.*, vol. 8, no. 1, pp. 458–468, Jan. 2023.

[19] Z. Liang, Z. Wang, J. Zhao, P. K. Wong, Z. Yang, and Z. Ding, "Fixed-time prescribed performance path-following control for autonomous vehicle with complete unknown parameters," *IEEE Trans. Ind. Electron.*, vol. 70, no. 8, pp. 8426–8436, Aug. 2023.

[20] J. Kim, H. Choi, and J. Kim, "A robust motion control with antiwindup scheme for electromagnetic actuated microrobot using time-delay estimation," *IEEE/ASME Trans. Mechatron.*, vol. 24, no. 3, pp. 1096–1105, Jun. 2019.

[21] J. Baek, S. Cho, and S. Han, "Practical time-delay control with adaptive gains for trajectory tracking of robot manipulators," *IEEE Trans. Ind. Electron.*, vol. 65, no. 7, pp. 5682–5692, Jul. 2018.

[22] C. Hu, Z. Wang, Y. Qin, Y. Huang, J. Wang, and R. Wang, "Lane keeping control of autonomous vehicles with prescribed performance considering the rollover prevention and input saturation," *IEEE Trans. Intell. Transp. Syst.*, vol. 21, no. 7, pp. 3091–3103, Jul. 2020.

[23] Z. Gao, Y. Zhang, and G. Guo, "Fixed-time prescribed performance adaptive fixed-time sliding mode control for vehicular platoons with actuator saturation," *IEEE Trans. Intell. Transp. Syst.*, vol. 23, no. 12, pp. 24176–24189, Dec. 2022.

[24] Z. Liang, J. Zhao, B. Liu, Y. Wang, and Z. Ding, "Velocity-based path following control for autonomous vehicles to avoid exceeding road friction limits using sliding mode method," *IEEE Trans. Intell. Transp. Syst.*, vol. 23, no. 3, pp. 1947–1958, Mar. 2022.

[25] K. Zhao, Y. Song, C. L. P. Chen, and L. Chen, "Adaptive asymptotic tracking with global performance for nonlinear systems with unknown control directions," *IEEE Trans. Autom. Control*, vol. 67, no. 3, pp. 1566–1573, Mar. 2022.

[26] V. Andrieu, L. Praly, and A. Astolfi, "Homogeneous approximation, recursive observer design, and output feedback," *SIAM J. Control Optim.*, vol. 47, no. 4, pp. 1814–1850, 2008.

[27] E. Cruz-Zavala and J. A. Moreno, "High-order sliding-mode control design homogeneous in the bi-limit," *Int. J. Robust Nonlinear Control*, vol. 31, no. 9, pp. 3380–3416, Jun. 2021.

[28] H. Q. Wang, B. Chen, and C. Lin, "Adaptive neural tracking control for a class of stochastic nonlinear systems," *Int. J. Robust Nonlinear Control*, vol. 24, no. 7, pp. 1262–1280, May 2014.

[29] Z. Zuo, "Nonsingular fixed-time consensus tracking for second-order multi-agent networks," *Automatica*, vol. 54, pp. 305–309, Apr. 2015.

[30] J. A. Moreno, "Arbitrary-order fixed-time differentiators," *IEEE Trans. Autom. Control*, vol. 67, no. 3, pp. 1543–1549, Mar. 2022.

[31] K. Youcef-Toumi and O. Ito, "A time delay controller for systems with unknown dynamics," *J. Dyn. Syst., Meas. Control*, vol. 112, no. 1, pp. 133–142, 1990.

Zhongchao Liang received the M.S. and Ph.D. degrees in mechanical engineering from the Harbin Institute of Technology, Harbin, China, in 2011 and 2015, respectively.

From 2019 to 2020, he was an Academic Visitor with the Department of Electrical and Electronic Engineering, The University of Manchester, Manchester, U.K. He is currently an Associate Professor with School of Mechanical Engineering and Automation, Northeastern University, Shenyang, China. His research interests include nonlinear and adaptive control for intelligent vehicles and mobile robots, and distributed control for multiagent systems.

Mingyu Shen received the B.S. degree in vehicle engineering from Beihua University, Jilin, China, in 2019, and the M.S. degree in transportation engineering from Northeast Forestry University, Harbin, China, in 2022. He is currently working toward the Ph.D. degree in mechanical engineering with School of Mechanical Engineering and Automation, Northeastern University, Shenyang, China.

His research interests include nonlinear control for intelligent vehicles and mobile robots.

Zhongguo Li (Member, IEEE) received the B.Eng. and Ph.D. degrees in electrical and electronic engineering from the University of Manchester, Manchester, U.K., in 2017 and 2021, respectively.

He was a Research Associate with the Department of Aeronautical and Automotive Engineering, Loughborough University, Loughborough, U.K. He is currently a Lecturer in robotics and AI with the Department of Computer Science, University College London, London, U.K. His research interests include optimization and decision-making for advanced control, game theory and learning in multiagent systems, and their applications in autonomous vehicles.

Jun Yang (Fellow, IEEE) received the B.Sc. degree in automation from the Department of Automatic Control, Northeastern University, Shenyang, China, in 2006, and the Ph.D. degree in control theory and control engineering from the School of Automation, Southeast University, Nanjing, China, in 2011.

He joined the Department of Aeronautical and Automotive Engineering, Loughborough University, Loughborough, U.K., in 2020, as a Senior Lecturer. His research interests include disturbance estimation and compensation, and advanced control theory and its application to mechatronic control systems and autonomous systems.

Dr. Yang was the recipient of the U.K. EPSRC New Investigator Award. He is an Associate Editor/Technical Editor for IEEE TRANSACTIONS ON INDUSTRIAL ELECTRONICS and IEEE-ASME TRANSACTIONS ON MECHATRONICS. He is a Fellow of IET.